Linear Nash perturbations with a CMB + Pantheon + $H(z)$ and BAO + DES Y1 joint analysis of cosmic growth expansion

Abraão J. S. Capistrano[*]

Universidade Federal do Paraná, 85950-000, Palotina-PR, Brazil
Federal University of Latin-American Integration, 85867-970 Foz do Iguaçu-PR, Brazil

We test a model associated with the Einstein gravity modified by using the linear Nash perturbations of the background metric. By means of a Markov chain Monte Carlo (MCMC) modeling, we combine the recent Dark Energy Survey (DES Y1) with the baryon acoustic oscillations (BAO) measurements and a larger datasets of "Gold 2018" growth data, the Planck 2018/ΛCDM parameters on the cosmic microwave background (CMB), the Pantheon Supernovae type Ia and the Hubble parameter data with redshift ranging from $0.01 < z < 2.3$ to derive the related constraints on the model parameters. We use the Jeffreys' scale to perform the Akaike information criterion (AIC) to ascertain the statistical viability of the model in comparison with the standard ΛCDM model. We find a mild reduction of the σ_8 discrepancy between the best-fit values of growth-rate amplitude factor and the matter content ($\sigma_8 - \Omega_m$) of the observations from CMB and large scale structure (LSS) probes. Due to the degeneracy of the model parameters, this situation may be improved. Oppositely, in the ΛCDM context, the situation is aggravated. For the considered large dataset, the discrepancy of best-fit values persists in both ($\sigma_8 - \Omega_m$) and ($h - \Omega_m$) planes and reinforces the mismatch of the Hubble parameter in CMB and BAO probes.

I. INTRODUCTION

In the face of the great challenges of gravitation, the possibility that the Universe might be embedded in extra dimensions reveals an interesting direction to follow. In particular, in a search of understanding the why of gravity is so weak in comparison with the other gauge fundamental interactions, the idea of extra dimensions criticizes the Planck regime that represents a very unpleasant combination of Newtonian gravity, special relativity and quantum mechanics. In the Newtonian context, gravity corresponds to the weak gravitational limit of general relativity theory (GR) and some indications tell that it holds up to 10^{-3} cm, with strong hints that it breaks down at 10^{-4} cm submillimeter scale [1–5]. In spite of these theoretical and experimental objections, the Planck regime is still regarded as an unshakable character of physical reality. In 1998, a new objection was risen by the seminal works of Arkani-Hamed, Dvali and Dimopolous (ADD) with the extra-dimensional ADD model [6], stating that the Planck regime lacks experimental support, i.e., it is not a verifiable hypothesis. This statement also applies to GR, to string theory loop quantum gravity, and many other models of quantum gravity. It seems that the simplest and most consistent way out of this dilemma is to change the

Planck scale itself by modifying the Newtonian gravitational constant G in the rhs of Einstein's equations.

Another seemingly unshakable landmark of standard gravitational physics is the Riemann geometry introduced in 1854. Let the tangent vectors be U and V, the Riemann curvature was defined by the linear transformation $R(U, V)W = [\nabla_U, \nabla_V]W - \nabla_{[U,V]}W$, where $[U, V]$ is the Lie brackets of the aforementioned tangent vectors. It characterizes the curvature of a manifold as compared with a flat manifold defined by $R(U, V) = 0$. However, the definition $R(U, V) = 0$ is ambiguous and quoted Riemann himself as saying "arbitrary cylindrical or conical surfaces (manifolds) count as equivalent to a plane" [7,8].

Fortunately, such ambiguity does not exist in GR because the Minkowski space-time is truly flat (i.e., a plane), as a consequence of the Poincaré symmetry. The importance of this stems from the fact that in GR the eigenvalues of the curvature tensor are the observables of the gravitational field, as compared with the Minkowski flat geometry. More than two decades ago, such comfortable situation changed, when observational evidences showed that there is a nonzero cosmological constant Λ. In cosmology, the simplest proposal for the explanation of the current accelerated regime is the well-known dark energy hypothesis, consisting in a sort of cosmological energy with negative pressure that speeds up the Universe. This is one of the pillars of the ΛCDM model regarded as the concordance cosmological model that considerably fits

[*]abecapistrano@gmail.com

well the most of the recent observations [9,10]. Even though its success, the lack of a fundamental understanding of its basic components, i.e, the cosmological constant Λ and the cold dark matter (CDM) constitute one of the cornerstone problems of this model [11–17].

To propose a different direction, the modified gravity by the extra-dimension corrections gives a different landscape of interesting possibilities. Most of these models have been Kaluza-Klein or/and string inspired, such as, for instance, the seminal works of the Arkani-Hamed, Dvali and Dimopolous (ADD) model [6], the Randall-Sundrum model [18,19] and the Dvali-Gabadadze-Porrati (DPG) model [20]. For instance, in the original DGP model, the space-time is a flat $(4 + 1)$-dimensional flat Minkowski and only gravity accesses the extra dimensions in the bulk space. The matter is trapped in the embedded space-time, the braneworld. The gravity is induced in a way that the DGP action relies on the addition of a five-dimensional bulk to a four-dimensional Einstein-Hilbert action. In particular, this scenario attracted much attention due to the possibilities to deal with, e.g., the accelerated expansion of the Universe and the hierarchy problem of fundamental interactions. In the self-accelerating branch, also known as sDGP, the DPG model is not coupled to any dark energy component but in the linearized theory, the model presents critical instabilities. In another direction, the normal branch (nDGP) associates the braneworld dynamics with a dark energy component to fit the observations with an advantage that the resulting models are ghost-free [21–25].

All in all, in those models and variants, the embedding of geometries is not properly developed. It is commonly fixed to a boundary in most models or particular conditions are needed to obtain their dynamics. On the other hand, several authors have been exploring the embedding of space-times as a promising mathematical structure for a physical theory [26–39]. Differently from ΛCDM and DPG models, the innovation of our proposal resides in a fully geometric mechanism based on the very foundations of differential geometry with a revival interest of curvature's concepts and on the necessity of a profound discussion of these foundations to the construction of a more general physical theory. The current problems posed by the contemporary cosmology are also related to the ΛCDM paradigm as a standard explanation for the accelerated expansion of the Universe. On the other hand, the presence of the cosmological constant Λ *per se* is an impediment to the existence of Minkowski space-time as a solution of Einstein's equations, representing the unique ground state of the gravitational field, favoring the de Sitter ground state. In addition, now we are faced to this ground state ambiguity that has its origin in the definition of the Riemann curvature. In a search of solving this ambiguity, we look at the conditions for the existence of the embedding of the space-time itself. The Nash-Greene [40,41] theorem is used to guarantee the geometrical stability as a solution of the embedding integrability conditions denoted by the Gauss, Codazzi and Ricci equations. The bulk acts as a reference geometry for the embedding. Hence, the dynamics is induced by the Nash-Greene perturbations of embedded space-time metric. The extrinsic curvature acts as a normal component for the gravitational field that accesses extra dimensions. This procedure is valid for any D dimensions [27–29]. For a physical model, this may lead to the necessary gravitational (amplified) sign of the classical Einstein's gravity; nonetheless a quantum approach of this model requires further development [29].

In this paper, we use the Nash-Greene embedding theorem [27–29,32–39] to develop a model under cosmological perturbations. We test the model by using a large pack of data to investigate the observed discrepancy of the best-fit points on the σ_8 contours revealed by the incompatibility of the data inferred from Planck CMB radiation and the large scale structure (LSS) observations. The σ_8 quantity measures the root-mean-square matter fluctuation within an enclosed mass of a sphere of radius $R \sim 8h$ Mpc^{-1} [42]. To constrain the cosmological parameters, we perform the Markov chain Monte Carlo (MCMC) sample technique as a tool for analyzing fit-to-data from a publicly available code [43–45] written in Wolfram *Mathematica*™ software. The joint likelihood is performed from the latest data on cosmic microwave background (CMB) radiation from Planck 2018 probe [10] compilation of the $(\text{TT}, \text{TE}, \text{EE} + \text{lowE} + \text{lensing})$ spectra within the 68% intervals for the best-fit parameters, the largest dataset of Pantheon SNIa [46] with redshift ranging from $0.01 < z < 2.3$, the Hubble parameter as a function of redshift $H(z)$ [47–52], the baryonic acoustic oscillations (BAO) and growth rate from using the data points of SDSS [53–55], 6dFGS [56], IRAS [57,58], 2MASS [57,59], 2dFGRS [60], GAMA [61], BOSS [62], WiggleZ [63], Vipers [64], FastSound [65], BOSS Q [66], the 2018 SDSS-IV [67–69] and the recent Dark Energy Survey one-year (DES Y1) based on galaxy clustering and weak gravitational lensing observations [70,71].

The paper is organized as follows: in the second section, we review the theoretical framework and its resulting cosmological model. In the third section, the main perturbed equations and the resulting growth equation are presented in a conformal Newtonian frame. The fourth section presents the outcomes and discussions from the comparison of the present model with ΛCDM of their cosmic growth expansion. The MCMC chain results are classified by the Akaike information criterion (AIC) [72] using the Jeffreys' scale for model selection. In the final section, we conclude with our remarks and future prospects. Concerning notation, we adopt the Landau timelike convention $(- - - +)$ for the signature of the four-dimensional embedded metric and speed of light $c = 1$. Capital Latin indices run from 1 to 5. Small case Latin indices refer to the only one extra dimension considered. All Greek indices refer to the embedded space-time counting from 1 to 4.

II. GEOMETRICAL ASPECTS

We start with the definition of the gravitational action in a D-dimensional ambient space (bulk) that has the form

$$S = -\frac{1}{2\kappa_D^2} \int \sqrt{|\mathcal{G}|} \mathcal{R} d^D x - \int \sqrt{|\mathcal{G}|} \mathcal{L}_m^* d^D x, \quad (1)$$

where κ_D^2 is the fundamental energy scale on the embedded space, $\mathcal{R}$ denotes de Ricci scalar of the bulk and $\mathcal{L}_m^*$ is the confined matter Lagrangian. Hence, the variation of Einstein-Hilbert action in Eq. (1) with respect to the bulk metric $\mathcal{G}_{AB}$ leads to the Einstein equations for the bulk

$$\mathcal{R}_{AB} - \frac{1}{2}\mathcal{G}_{AB} = \alpha^\star \mathcal{T}_{AB}, \quad (2)$$

where $\alpha^\star$ is energy scale parameter and $\mathcal{T}_{AB}$ is the energy-momentum tensor for the bulk [28,29,32].

Let us consider a Riemannian manifold V_4 with a nonperturbed metric $\bar{g}_{\mu\nu}$ being locally and isometrically embedded in an n-dimensional Riemannian manifold V_n given by a differentiable and regular map $\mathcal{X}: V_4 \to V_n$ satisfying the embedding equations [40,41]

$$\mathcal{X}_{,\mu}^A \mathcal{X}_{,\nu}^B \mathcal{G}_{AB} = \bar{g}_{\mu\nu}, \quad (3)$$

$$\mathcal{X}_{,\mu}^A \bar{\eta}_a^B \mathcal{G}_{AB} = 0, \quad (4)$$

$$\bar{\eta}_a^A \bar{\eta}_b^B \mathcal{G}_{AB} = \bar{g}_{ab}, \quad (5)$$

where $\mathcal{G}_{AB}$ denotes the metric components of V_n in arbitrary coordinates and $\bar{\eta}$ denotes a nonperturbed unit vector field orthogonal to V_4. This set of equations represents the isometry condition Eq. (3), in Eq. (4) sets the orthogonality between the embedding coordinates $\mathcal{X}$ and $\bar{\eta}$, and also, in Eq. (5), one has the vector normalization $\bar{\eta}$ and $\bar{g}_{ab} = \epsilon_a \delta_{ab}$ with $\epsilon_a = \pm 1$ that the signs represent the signatures of the extra dimensions. In this particular case, we have a model with only one extra dimension. Hence, the integration of the system of equations [Eqs. (3)–(5)] sets the embedding map $\mathcal{X}$.

The nonperturbed extrinsic curvature $\bar{k}_{\mu\nu}$ of V_4 is defined as the projection of the variation of $\bar{\eta}$ onto the tangent plane,

$$\bar{k}_{\mu\nu} = -\mathcal{X}_{,\mu}^A \bar{\eta}_{,\nu}^B \mathcal{G}_{AB} = \mathcal{X}_{,\mu\nu}^A \bar{\eta}^B \mathcal{G}_{AB}, \quad (6)$$

where the comma denotes the ordinary derivative.

To obtain the embedded four-dimensional equations in a five-dimensional space-time, one can take Eq. (2) written in the Gaussian frame embedding veilbein $\{\mathcal{X}_\mu^A, \bar{\eta}_a^A\}$. This reference frame is composed by a regular and differentiable coordinate $\{\mathcal{X}^A\}$ and a unitary normal vector $\{\bar{\eta}_a^A\}$. Accordingly, they define the basis of the embedded geometry and one can obtain the embedded four-dimensional field equations for the background,

$$R_{\mu\nu} - \frac{1}{2}Rg_{\mu\nu} + \bar{Q}_{\mu\nu} = 8\pi G\bar{T}_{\mu\nu}, \quad (7)$$

$$\bar{k}_{\mu;\rho}^\rho - h_{,\mu} = 0, \quad (8)$$

where G denotes the Newtonian gravitational constant. In Eq. (8) we have the trace of Codazzi equations and the mean Gaussian curvature is denoted by $h = \bar{g}^{\mu\nu}\bar{k}_{\mu\nu}$ and $h^2 = h.h$. The semicolon denotes the ordinary covariant derivative. The background energy-momentum tensor is denoted by $\bar{T}_{\mu\nu}$. The D-dimensional case was discussed in former works as in Refs. [27–32,39].

A. Background equations and results

The Friedmann-Lemaître-Robertson-Walker (FLRW) metric in coordinates (r, θ, ϕ, t) gives the evolution of an embedded four-dimensional cosmology as

$$ds^2 = dt^2 - a^2[dr^2 + f_\kappa^2(r)(d\theta^2 + \sin^2\theta d\varphi^2)], \quad (9)$$

where $a \equiv a(t)$ is the scale expansion factor and $f(r)_\kappa = \sin r$, r,$\sinh r$. Moreover, κ corresponds to spatial curvature $(1, 0, -1)$. In this paper, we consider a flat universe with $\kappa = 0$ in accordance with recent observations [10].

The four-dimensional nonperturbed energy-momentum tensor of a perfect fluid $\bar{T}_{\mu\nu}$ is defined in comoving coordinates as

$$\bar{T}_{\mu\nu} = (\bar{p} + \bar{\rho})U_\mu U_\nu + \bar{p}\bar{g}_{\mu\nu}, \qquad U_\mu = \delta_\mu^4, \quad (10)$$

where U_μ is the comoving four-velocity and the related conservation equation is given by

$$\bar{\rho} + 3H(\bar{\rho} + \bar{p}) = 0, \quad (11)$$

where ρ and p denote nonperturbed matter density and pressure, respectively. The Hubble parameter is defined as usual in terms of the expansion factor a as $H \equiv H(t) = \frac{\dot{a}}{a}$. The dot symbol denotes the ordinary time derivative. It is important to stress that the related matter gauge interactions are confined in the embedded four-dimensional space-time [73–75]. As a result of the embedding, the nonperturbed deformation tensor $\bar{Q}_{\mu\nu}$ is an entirely geometrical term given by

$$\bar{Q}_{\mu\nu} = \bar{g}^{\rho\sigma}\bar{k}_{\mu\rho}\bar{k}_{\nu\sigma} - \bar{k}_{\mu\nu}h - \frac{1}{2}(K^2 - h^2)\bar{g}_{\mu\nu}, \quad (12)$$

where the term $K^2 = \bar{k}^{\mu\nu}\bar{k}_{\mu\nu}$ is the Gaussian curvature. It is important to note that the deformation tensor $Q_{\mu\nu}$ is conserved in such a way:

$$\bar{Q}_{\mu\nu;\nu} = 0. \quad (13)$$

From the spatially flat FLRW metric in Eq. (9), we obtain a solution of Eq. (8) with the following components:

$$\bar{k}_{ij} = \frac{b}{a^2}\bar{g}_{ij}, i, \quad j = 1, 2, 3, \quad \bar{k}_{44} = \frac{-1}{\dot{a}}\frac{d}{dt}\frac{b}{a},$$

where a is the usual expansion parameter and $b(t) \equiv b = k_{11}$ is the bending function. Analogously to the definition of the Hubble parameter H, we define the extrinsic function $B \equiv B(t) = \dot{b}/b$. From Ref. [32], we summarize the background quantities by direct calculation of Eqs. (7) and (8) as

$$\bar{k}_{44} = -\frac{b}{a^2}\left(\frac{B}{H} - 1\right), \tag{14}$$

$$K^2 = \frac{b^2}{a^4}\left(\frac{B^2}{H^2} - 2\frac{B}{H} + 4\right), \qquad h = \frac{b}{a^2}\left(\frac{B}{H} + 2\right) \tag{15}$$

$$\bar{Q}_{ij} = \frac{b^2}{a^4}\left(2\frac{B}{H} - 1\right)\bar{g}_{ij}, \qquad \bar{Q}_{44} = -\frac{3b^2}{a^4}, \tag{16}$$

$$\bar{Q} = -(K^2 - h^2) = \frac{6b^2}{a^4}\frac{B}{H}, \tag{17}$$

where in Eq. (16), we have denoted $i, j = 1\ldots3$, with no sum on indices. Thus, the bending function $b(t)$ can be written as

$$b(t) = \alpha_0 a^{\beta_0}, \tag{18}$$

where α_0 and β_0 denote integration constants. With additional information gained by means of calculating $\bar{Q}_{ij;i} = 0$, assuming $B/H = $ constant, and using the FLRW coordinates, one obtains the Friedman equation modified by the extrinsic curvature as

$$\left(\frac{\dot{a}}{a}\right)^2 = \frac{8}{3}\pi G\bar{\rho} + \alpha_0 a^{2\beta_0 - 4}. \tag{19}$$

When $\alpha_0 \to 0$, the GR limit is obtained with the reproduction of the standard first Friedmann equation. The ΛCDM limit is also obtained with $\alpha_0 \to 0$ plus the consideration of the vacuum energy density ρ_Λ in the total energy density. In this study, we consider the total energy density $\bar{\rho}$ is given by $\bar{\rho} = \bar{\rho}_{mat} + \bar{\rho}_{rad}$, where we denote the matter ρ_{mat} and radiation energy ρ_{rad} densities, respectively. Based on previous cosmography tests [32,34–36,38], the parameter β_0 measures the range of the magnitude of the deceleration parameter $q(z)$ in function of the redshift z, where the standard relation with the expansion parameter $a = \frac{1}{1+z}$ applies. Thus, the resulting model is defined by Hubble evolution $H(z)$ as

$$H(z) = H_0\sqrt{\Omega_m(z) + \Omega_{rad}(z) + \Omega_{ext}(z)}, \tag{20}$$

where $H(z)$ is the Hubble parameter in terms of redshift z and H_0 is the current value of the Hubble constant. The matter density parameter is denoted by $\Omega_m(z) = \Omega_{m0}(1 + z)^3$,

$\Omega_{rad}(z) = \Omega_{rad0}(1 + z)^4$ with $\Omega_{rad0} = \Omega_{m0}z_{eq}$ and the term $\Omega_{ext}(z) = \Omega_{ext0}(1 + z)^{4-2\beta_0}$ stands for the density parameter associated with the extrinsic curvature. The subscript "0" indicates the present value of any quantity. The equivalence number for the expansion factor a_{eq} given by

$$a_{eq} = \frac{\Omega_\gamma + \Omega_\nu}{\Omega_{m0}}, \tag{21}$$

where Ω_γ is the photon density distribution given by

$$\Omega_\gamma = \frac{\pi^2}{30}g_\gamma\frac{T^4}{\rho_{cr}}, \tag{22}$$

where the critical density $\rho_{cr} = 8.098 \times 10^{-11}h^2$ eV^4 and the CMB temperature is adopted for the value $T_{cmb} = 2.7255K$, with one Kelvin $K = 8.621738 \times 10^{-5}$ eV, and the factor $g_\gamma = 2$. The neutrino species are denoted by Ω_ν:

$$\Omega_\nu = N_{eff}\frac{7}{8}\left(\frac{4}{11}\right)^{4/3}\Omega_\gamma, \tag{23}$$

where N_{eff} is the effective number of neutrinos and the adopted value is $N_{eff} = 3.046$.

The current extrinsic contribution Ω_{ext0} is given by the normalization condition for redshift at $z = 0$ that results in

$$\Omega_{ext}^0 = (1 - \Omega_{m0} - \Omega_{rad0}). \tag{24}$$

Hence, we can write the dimensionless Hubble parameter $E(z)$ for a flat universe as

$$E^2(z) = \Omega_{m0}(1 + z)^3 + \Omega_{rad0}(1 + z)^4$$
$$+ (1 - \Omega_{m0} - \Omega_{rad0})(1 + z)^{4-2\beta_0}. \tag{25}$$

The ΛCDM analogy is obtained with setting $\beta_0 = 2$. Hereon, the present model is referred to as β-model only to facilitate the referencing.

III. PERTURBED EQUATIONS IN CONFORMAL NEWTONIAN GAUGE

In longitudinal conformal Newtonian gauge, the metric in Eq. (9) is given by

$$ds^2 = a^2[(1 + 2\Phi)d\eta^2 - (1 - 2\Psi)\delta_{ij}dx^i dx^j], \tag{26}$$

where $\Phi = \Phi(\vec{x}, \eta)$ and $\Psi = \Psi(\vec{x}, \eta)$ denotes the Newtonian potential and the Newtonian curvature, respectively. The conformal time η is related with physical time as $dt = a(\eta)d\eta$.

The perturbed field equations of Eqs. (7) and (8) can be written as

$$\delta G_{\mu\nu} + \delta Q_{\mu\nu} = 8\pi G\delta T_{\mu\nu}, \tag{27}$$

$$\delta k_{\mu\nu;\rho} = \delta k_{\mu\rho;\nu}. \tag{28}$$

Hereon the background quantities are represented by the tilde symbol.

To obtain the explicit form for perturbed field equations in Eqs. (27) and (28), we need to determine both perturbed metric $\delta g_{\mu\nu}$ and perturbed extrinsic curvature $\delta k_{\mu\nu}$. Using the main result of the Nash-Greene theorem [40,41] that warrants the perturbations of the embedded space-time through a smoothing differentiable process and the bulk stability, one can use the relation

$$\delta g_{\mu\nu} = -2\bar{k}_{\mu\nu}\delta y, \tag{29}$$

where δy denotes an infinitesimal displacement of the extra dimension y in the bulk space. It is important to point out that the y variable is not considered in the line elements like that of rigid embedding models [18–20] since it is implicitly applied in the perturbation process. To see how it happens, consider a linear perturbation of a new geometry $g_{\mu\nu}$ is given by $g_{\mu\nu} = \bar{g}_{\mu\nu} + \delta g_{\mu\nu}$ that can be written as

$$g_{\mu\nu} = \bar{g}_{\mu\nu} - 2\delta y\bar{k}_{\mu\nu}, \tag{30}$$

and the related perturbed extrinsic curvature

$$k_{\mu\nu} = \bar{k}_{\mu\nu} - 2\delta y\bar{g}^{\sigma\rho}\bar{k}_{\mu\sigma}\bar{k}_{\nu\rho}, \tag{31}$$

where we can identify $\delta k_{\mu\nu} = -2\delta y\bar{g}^{\sigma\rho}\bar{k}_{\mu\sigma}\bar{k}_{\nu\rho}$. Using the Nash relation $\delta g_{\mu\nu} = -2\bar{k}_{\mu\nu}\delta y$, we obtain

$$\delta k_{\mu\nu} = \bar{g}^{\sigma\rho}\bar{k}_{\mu\sigma}\delta g_{\nu\rho}. \tag{32}$$

From Eqs. (12) and (32), one obtains the perturbation of the deformation tensor $Q_{\mu\nu}$:

$$\delta Q_{\mu\nu} = -\frac{3}{2}(K^2 - h^2)\delta g_{\mu\nu}. \tag{33}$$

Like the nonperturbed conservation of $\bar{Q}_{\mu\nu}$ in Eq. (13), the perturbed $\delta Q_{\mu\nu}$ is also independently conserved in a sense that $\delta Q_{\mu\nu;\nu} = 0$. Accordingly, using the background relations in Eqs. (14)–(17), it is straightforward to determine the components of $\delta Q_{\mu\nu}$:

$$\delta Q_{ij} = \gamma_0 a^{2\beta_0 - 2}\Psi\delta^i_j, \tag{34}$$

$$\delta Q_{i4} = 0, \tag{35}$$

$$\delta Q_{44} = \gamma_0 a^{2\beta_0 - 2}\Phi\delta^4_4, \tag{36}$$

where we denote $\gamma_0 = k_0\alpha_0$. The term k_0 is an integration constant and α_0 is a constant originated from integrating the bending function $b(t)$ in Eq. (18).

As a preliminary study on cosmic perturbations of the present model, we do not consider an anisotropic fluid-pressure contribution to analyze a clean gravitational sign originated from the extrinsic part. Hence, likewise GR, for a pressureless and null anisotropic matter stresses, we obtain the simplest condition for perturbations for the potentials in such an equality $\Psi = \Phi$. As a result, one obtains the following set of equations in the wave number k-space of Fourier modes simply as

$$k^2\Phi_k + 3\mathcal{H}(\Phi'_k + \Phi_k\mathcal{H}) = -4\pi Ga^2\delta\rho_k + 9\gamma_0 a^{2\beta_0}\Phi_k, \tag{37}$$

$$\Phi''_k + 3\mathcal{H}\Phi'_k + (\mathcal{H}^2 + 2\mathcal{H}')\Phi_k = 9\gamma_0 a^{2\beta_0}\Phi_k,$$

where $\mathcal{H} \equiv aH$. In the aforementioned equations, when $\gamma_0 \to 0$, the standard GR equations are restored. Moreover, we obtain a relation of Φ_k and δ_m as

$$k^2\Phi_k = -4\pi G_{\text{eff}}a^2\bar{\rho}\delta_m, \tag{38}$$

where G_{eff} is the effective Newtonian constant and is given by

$$G_{\text{eff}}(a, k) = \frac{G}{1 - \frac{\gamma_0}{k^2}a^{2\beta_0}}, \tag{39}$$

where G is the Newtonian gravitational constant.

The corresponding equation of evolution of the contrast matter density $\delta_m(\eta)$ in conformal longitudinal Newtonian frame can be written as

$$\delta''_m + \mathcal{H}\delta'_m - 4\pi G_{\text{eff}}a^2\bar{\rho}\delta_m = 0, \tag{40}$$

where the prime symbols denote derivatives with respect to conformal time η. Alternatively, one obtains the contrast matter density $\delta_m(a)$ in terms of the expansion factor $a(t)$ as

$$\ddot{\delta}_m(a) + \left(\frac{3}{a} + \frac{\dot{H}(a)}{H(a)}\right)\dot{\delta}_m(a) - \frac{3\Omega_{m0}G_{\text{eff}}/G}{2(H^2(a)/H_0^2)}\delta_m(a) = 0, \tag{41}$$

where the dot symbols denote derivatives with respect to scale factor a.

IV. OBSERVATIONAL CONSTRAINTS: ANALYSIS AND RESULTS

A. Statistical considerations on the data

In this section, we summarize the main statistical tools used for analyzing the observational data on growth fluctuations, CMB Planck 2018 data, BAO with additional DES Y1 data and the large Pantheon SNIa. A complete set and description of these formulas can be found in detail in Refs. [43–45,76,77].

1. Growth-rate fluctuations

The data on growth-rate fluctuations is used by working with the σ_8 parameter that measures the growth of rms fluctuations on the $8h^{-1}$ Mpc scale. This is performed by the definition of the quantity

$$f\sigma_8(a) \equiv f(a)\,\sigma_8(a), \qquad (42)$$

where $f(a) = \frac{\ln\delta}{\ln a}$ is the growth rate and the growth factor $\delta(a)$ is given by Eq. (41). To compatibilize the data dependence from the fiducial cosmology and another cosmological survey, it is necessary to rescale the growth-rate data by the ratio $r(z)$ of the Hubble parameter $H(z)$ and the angular distance $d_A(z)$ by the quantity

$$r(z) = \frac{H(z)d_A(z)}{H_f(z)D_f A(z)}, \qquad (43)$$

where the subscript "f" corresponds to some quantity of fiducial cosmology. Accordingly, the angular distance $d_A(z)$ is defined as

$$d_A(z) = \frac{c}{(1+z)} \int_z^0 \frac{1}{H(z')}\,dz'. \qquad (44)$$

Likewise, the regulation of the χ^2 statistics is also necessary that relies on a general definition

$$\chi^2(\Omega_{m0}, w, \beta_0, \gamma_0, \sigma_8) = V^i C_{ij}^{-1} V_j, \qquad (45)$$

where $V^i \equiv f\sigma_{8,i} - r(z_i)f\sigma_8(z_i, \Omega_{m0}, w, \beta_0, \gamma_0, \sigma_8)$ denotes a set of vectors that go up to ith data points at redshift z_i for each $i = 1\ldots N$. N is the total number of data points of a related collection of data. The set of $f\sigma_{8,i}$ data points comes from theoretical predictions [43]. The set of C_{ij}^{-1} denotes the inverse covariance matrix. A final important correction concerns the necessity to disentangle the data points related to the WiggleZ dark energy survey which are at first correlated. Then, the covariant matrix C_{ij} [63] is given by

$$C_{ij}^{\text{wigglez}} = 10^{-3} \begin{pmatrix} 6.400 & 2.570 & 0.000 \\ 2.570 & 3.969 & 2.540 \\ 0.000 & 2.540 & 5.184 \end{pmatrix}, \qquad (46)$$

and the resulting total matrix C_{ij}^{tot}

$$C_{ij}^{\text{tot}} = 10^{-3} \begin{pmatrix} \sigma_1^2 & 0 & 0 & \cdots \\ 0 & C_{ij}^{\text{wigglez}} & 0 & \cdots \\ 0 & 0 & \cdots & \sigma_N^2 \end{pmatrix}, \qquad (47)$$

where the set of σ^2's denotes the N variances.

2. CMB radiation from Planck 2018 data

For the CMB radiation data, we used the Planck 2018 released [10] with χ^2 statistics:

$$\chi_{\text{CMB}}^2 = X_{\text{Planck2018}}^T C_{\text{CMB}}^{-1} X_{\text{Planck2018}}, \qquad (48)$$

where the covariant matrix for the parameters for $R, l_A, \Omega_{b0}h^2$ is given by

$$X_{\text{Plankc2018}} = \begin{pmatrix} R - 1.7502 \\ l_A - 301.471 \\ \omega_b - 0.02236 \end{pmatrix}, \qquad (49)$$

where $\omega_b = \Omega_{b0}h^2$. The two shift parameters R and l_A are defined as the scale distance and acoustic scale,

$$R = \frac{\sqrt{\Omega_{m0}}}{c}\,d_A(z_{\text{CMB}})(1 + z_{\text{CMB}}), \qquad (50)$$

$$l_A = \frac{\pi d_A(z_{\text{CMB}})(1 + z_{\text{CMB}})}{r_s(z_{\text{CMB}})}, \qquad (51)$$

where the angular distance d_A is given by Eq. (44) and the related redshift at recombination z_{CMB} is given by

$$z_{\text{CMB}} = 1048[1 + 0.00124(\Omega_b h^2)^{-0.738}][1 + g_1(\Omega_{m0}h^2)^{g_2}], \qquad (52)$$

and the parameters g_1, g_2 are defined accordingly, as

$$g_1 = \frac{0.0783(\Omega_b h^2)^{-0.238}}{1 + 39.5(\Omega_b h^2)^{0.763}}; \qquad g_2 = \frac{0.560}{1 + 21.1(\Omega_b h^2)^{1.81}}. \qquad (53)$$

The comoving sound horizon $r_s(z)$ is given by

$$r_s(z) = c \int_z^\infty \frac{c_s(z')}{H(z')}\,dz', \qquad (54)$$

and the related sound speed c_s

$$c_s(z) = \frac{1}{\sqrt{3(1 + \bar{R}_b/(1+z))}}, \qquad (55)$$

with $\bar{R}_b = 31500\Omega_{b0}h^2(T_{\text{CMB}}/2.7K)^{-4}$. Moreover, the inverse of the covariant matrix C_{CMB}^{-1} for the parameters for $l_a, R, \Omega_{b0}h^2$ is given by $C_{\text{CMB}}^{-1} = \sigma_i\sigma_j C$, with $\sigma_i = (0.0046, 0.090, 0.00015)$ for the normalized covariance matrix given by

$$C = \begin{pmatrix} 1.00 & 0.46 & -0.66 \\ 0.46 & 1.00 & -0.37 \\ -0.66 & -0.33 & 1.00 \end{pmatrix}. \qquad (56)$$

3. BAO joint data

In a similar manner, we summarize some the useful formulas to work with BAO from the set of probes on SDSS [53–55], 6dFGS [56], IRAS [57,58], 2MASS [57,59], 2dFGRS [60], GAMA [61], BOSS [62], WiggleZ [63], Vipers [64], FastSound [65], BOSS Q [66] and additional points from the 2018 SDSS-IV [67–69].

We use the χ^2 statistics for WiggleZ in a form

$$\chi^2_{\text{WiggleZ}} = (\bar{A}_{\text{obs}} - \bar{A}_{th})C^{-1}_{\text{WiggleZ}}(\bar{A}_{\text{obs}} - \bar{A}_{th})^T, \quad (57)$$

where $\bar{A}_{\text{obs}} = (0.447, 0.442, 0.424)$ refers to the data vectors at $z = (0.44, 0.60, 0.73)$ and the acoustic scale parameter $\bar{A}_{th} = (z, p_i)$ as defined in [78], is calculated as

$$\bar{A}_{th} = D_V(z)\frac{\sqrt{\Omega_{m0}H_0^2}}{cz}, \quad (58)$$

and does not depend on a related dark energy model. The dilation scale D_V was defined by [78] and is a geometric mean between the transverse and radial directions used to distinguish the BAO features separately in angular and radial line-of-sight directions since from galaxy redshift surveys these features are mostly mixed up [79]. Then, the dilation scale D_V is given by the relation

$$D_V(z) = \frac{1}{H_0}\left[(1+z)^2 d_A(z)^2 \frac{cz}{E(z)}\right]^{1/3}. \quad (59)$$

Moreover, the inverse of the covariant matrix C^{-1}_{WiggleZ} is

$$C^{-1}_{\text{WiggleZ}} = \begin{pmatrix} 1040.3 & -807.5 & 336.8 \\ -807.5 & 3720.3 & -1551.9 \\ 336.8 & -1551.9 & 2914.9 \end{pmatrix}. \quad (60)$$

Like the previous case, we adopt the same analysis on SDSS data such as

$$\chi^2_{\text{SDSS}} = (\bar{d}_{\text{obs}} - \bar{d}_{th})C^{-1}_{\text{SDSS}}(\bar{d}_{\text{obs}} - \bar{d}_{th})^T, \quad (61)$$

where $\bar{d}_{\text{obs}} = (0.1905, 0.1097)$ refers to the data vectors at $z = (0.2, 0.35)$. The quantity $\bar{d}_{th}$ denotes a model-independent quantity given by the ratio

$$\bar{d}_{th} = \frac{r_s(z_d)}{D_V(z)}, \quad (62)$$

where the related comoving sound horizon $r_s(z)$ and dilation scale $D_V(z)$ were given previously by Eqs. (54) and (59), respectively. Such distance redshift relation is important to constrain BAO measurements from galaxy surveys as standard rulers. In addition, the drag redshift is defined as

$$z_{\text{drag}} = \frac{1291(\Omega_m h^2)^{0.251}}{1 + 0.659(\Omega_m h^2)^{0.828}}[1 + b_1(\Omega_m h^2)^{b_2}], \quad (63)$$

where $b_1 = 0.313(\Omega_m h^2)^{-0.419}[1 + 0.607(\Omega_m h^2)^{0.674}]$ and $b_2 = 0.238(\Omega_m h^2)^{0.223}$. It is important to point out that the so-called drag epoch marks the photons and baryons decoupling from the last scattering of CMB photons and the related z_{drag} marks when the baryon-drag optical depth equals unity. The inverse of the covariant matrix C^{-1}_{SDSS} is given by

$$C^{-1}_{\text{SDSS}} = \begin{pmatrix} 30124 & -17227 \\ -17227 & 86977 \end{pmatrix}. \quad (64)$$

For the DES Y1 data [70,71], the likelihood $\mathcal{L}_{\text{DES}}(\alpha) \propto e^{-\chi^2(\alpha)/2}$ is calculated directly from the angular scale $d_A(z)$ and the comoving sound horizon $r_s(z)$ by the scale dilation α-parameter that accounts for deviations from the fiducial cosmology such as

$$\alpha = \frac{d_A(z_{\text{eff}})r^{\text{fid}}(z_{\text{drag}})}{d_A^{\text{fid}}(z_{\text{eff}})r(z_{\text{drag}})}, \quad (65)$$

where $r(z_{\text{drag}})_{\text{fid}} = 153.44$ Mpc and for the Y1 measurements, the effective redshift $z_{\text{eff}} = 0.81$ and $d_A(z_{\text{eff}})/r(z_{\text{drag}}) = 10.75 \pm 0.43$ adding three data point numbers to the overall BAO contribution. The total χ^2_{BAO} is obtained from the sum of the individual χ^2 of each dataset.

4. The Pantheon supernova type Ia data

We determine the theoretical distance modulus $\mu_{th}(z)$ to obtain the constraints from SNIa given by

$$\mu_{th}(z) = 5\log_{10}(d_L(z)) + \mu_0, \quad (66)$$

where $\mu_0 = 42.38 - 5\log_{10}\mathbf{h}$ and $\mathbf{h} = 0.672$. The luminosity distance d_L related to the Hubble expansion rate is given by

$$d_L(z|s, \mu_0) = (1+z)\int_0^z \frac{du}{E(u|s)}, \quad (67)$$

where s denotes the free parameters of a model. We use the prior for the density parameter of visible baryonic matter $\Omega_{b0} = 2.236/100\mathbf{h}^2$. The χ^2 statistics are used in a form

$$\chi^2_{SnIa}(s|\mu_0) = \sum_{i=1}^n \frac{[\mu_{th,i}(s, \mu_0|z_i) - \mu_{obs,i}(z_i)]}{\sigma^2_{\mu i}}, \quad (68)$$

where $n = 1048$ is the number of events of the Pantheon SNIa data [46], the distance modulus obtained from observations is denoted by $\mu_{obs,i}(z_i)$, and $\sigma_{\mu i}$ is the total uncertainty of the observational data.

TABLE I. CMB Planck 2018/ΛCDM cosmological parameters of the 68% intervals from TT, TE, EE + lowE + lensing spectra [10].

Parameter	Best fits
Ω_{m0}	0.3153 ± 0.0073
$\Omega_{b0}h^2$	2.237 ± 0.015
H_0 [kms^{-1} Mpc^{-1}]	67.36 ± 0.540
σ_8	0.8111 ± 0.0060

TABLE II. Data points of the "extended Gold-2018" growth-rate compilation [43] with additional points from BOSS Q [66] and SSSD-IV [67–69].

Dataset	Redshift	$f\sigma_8(z)$	Ω_m
6dFGS + SnIa	0.02	0.428 ± 0.0465	0.3
SnIa + IRAS	0.02	0.398 ± 0.065	0.3
2MASS	0.02	0.314 ± 0.048	0.266
SDSS-veloc	0.10	0.370 ± 0.130	0.3
SDSS-MGS	0.15	0.490 ± 0.145	0.31
2dFGRS	0.17	0.510 ± 0.060	0.3
GAMMA	0.18	0.360 ± 0.090	0.27
GAMMA	0.38	0.440 ± 0.090	0.27
SDSS-LRG-200	0.25	0.3512 ± 0.0583	0.25
SDSS-LRG-200	0.37	0.4602 ± 0.0378	0.25
BOSS-LOWZ	0.32	0.384 ± 0.095	0.274
SDSS-CMASS	0.59	0.488 ± 0.060	0.30711
WiggleZ	0.44	0.413 ± 0.080	0.27
WiggleZ	0.60	0.390 ± 0.063	0.27
WiggleZ	0.73	0.437 ± 0.072	0.27
Vipers PDR-2	0.60	0.550 ± 0.120	0.3
Vipers PDR-2	0.86	0.400 ± 0.110	0.3
FastSound	1.40	0.482 ± 0.116	0.270
BOSS-Q	1.52	0.426 ± 0.077	0.31
SDSS-IV	1.52	0.420 ± 0.076	0.26479
SDSS-IV	1.52	0.396 ± 0.079	0.31
SDSS-IV	0.978	0.379 ± 0.176	0.31
SDSS-IV	1.23	0.385 ± 0.099	0.31
SDSS-IV	1.526	0.342 ± 0.070	0.31
SDSS-IV	1.944	0.364 ± 0.106	0.31

B. Results and discussion

The methodology used in this paper relies on the Markov chain Monte Carlo (MCMC) sample technique adapted from the publicly available code of a modified MetropolisHastings algorithm [44,45] to infer the parameter likelihoods. We perform our analysis using the joint likelihood of kinematical probes on the CMB Planck 2018 data [10] of the (TT, TE, EE + lowE + lensing) spectra within the 68% intervals of the best-fit parameters as shown in Table I, the Pantheon SNIa [46] with redshift ranging from $0.01 < z < 2.3$, the Hubble parameter $H(z)$ as a function of redshift [47–52], BAO and growth-rate compilation using data points of SDSS [53–55], 6dFGS [56], IRAS [57,58], 2MASS [57,59], 2dFGRS [60], GAMA [61], BOSS [62], WiggleZ [63], Vipers [64], FastSound [65], BOSS Q [66], the SSSD-IV 2018 data [67–69] and three more data points from the DES Y1 collaboration [70,71].

To apply our χ^2-statistics, we extract the data points from the Pantheon SNIa, CMB, BAO, Hubble parameter and growth, with the amount of 1048, 3, 12, 36 and 25 data points, respectively, with a total of 1124 data points. In order to keep the analysis on the subhorizon linear scale, we set the minimum value of expansion parameter as $a_{\min} = 0.001$ and $k = 300H_0 \sim 0.1h$ Mpc^{-1}. We use the parameter vectors for the β-model as $\{\Omega_{m0}, 100\Omega_b h^2, h, \beta_0, \gamma_0, \sigma_8\}$ with the adopted priors $\{(0.001, 1), (0.001, 0.08), (0.4, 1), (1.9, 2.001), (0.999, 1.001), (0.1, 1.8)\}$. For ΛCDM, we set the vectors and priors $\{\Omega_{m0}, 100\Omega_b h^2, h, \sigma_8\}$ with $w = -1$ and $\{(0.001, 1), (0.001, 0.08), (0.4, 1), (0.1, 1.8)\}$. To the CMB temperature, we adopt a reference value of $T_{\rm cmb} = 2.7255K$. Moreover, the joint analysis was also implemented by the product of the particular likelihoods $\mathcal{L}$ for each data set

$$\mathcal{L}_{\rm tot} = \mathcal{L}_{\rm Pantheon}.\mathcal{L}_{\rm BAO}.\mathcal{L}_{\rm CMB}.\mathcal{L}_{H(z)}.\mathcal{L}_{\rm growth} \quad (69)$$

and the sum of individual χ^2 to get the total χ^2:

$$\chi^2_{\rm tot} = \chi^2_{\rm Pantheon} + \chi^2_{\rm BAO} + \chi^2_{\rm CMB} + \chi^2_{H(z)} + \chi^2_{\rm growth}. \quad (70)$$

The list of full values for the $H(z)$ data can be found in Tables (1) and (2) of Ref. [45]. Moreover, in Tables III and IV, we present the best-fit and median values for the studied models.

To proceed further, more information can be obtained by the contours of the main cosmological parameters. In Fig. 1, we show the results of contours from the MCMC chains of the cosmological parameters for the ΛCDM model with the related probability density function

TABLE III. A summary of best-fit values of the background parameters calculated by using MCMC chains with the resulting χ^2 values. The χ^2_{bf} denotes the χ^2 best-fit values from MCMC chains and $\chi^2_{\rm red}$ refers to reduced χ^2 from the value of the total χ^2 of minimizing all data and the related degrees of freedom. Errors were obtained directly from the covariant matrix of the MCMC chains.

Model	Ω_{m0}	$100\Omega_{b0}h^2$	h	σ_8	Parameters	$\chi^2_{\rm red}$	χ^2_{bf}
ΛCDM	0.311 ± 0.006	2.242 ± 0.014	0.679 ± 0.005	0.759 ± 0.034	$w = -1$	0.972	1088.29
β-model	0.312 ± 0.007	2.240 ± 0.014	0.680 ± 0.006	0.765 ± 0.027	$\beta_0 = 1.999 \pm 0.025$ $\gamma_0 = 1.001 \pm 0.016$	0.973	1088.34

TABLE IV. A summary of median values of background parameters calculated by using MCMC chains of the main parameters.

Model	Ω_{m0}	$100\Omega_{b0}h^2$	h	σ_8	Parameters
ΛCDM	0.311 ± 0.004	2.242 ± 0.010	0.679 ± 0.003	0.754 ± 0.020	$w = -1$
β-model	0.316 ± 0.005	2.244 ± 0.010	0.673 ± 0.004	0.760 ± 0.020	$\beta_0 = 1.961 \pm 0.020$ $\gamma_0 = 1.022 \pm 0.013$

(PDF). Particularly, the $(\sigma_8 - \Omega_m)$ and $(h - \Omega_m)$ planes show a discrepancy between the obtained median values (black points) of the ΛCDM model and the best-fit values from the Planck 2018 (TT + TE + EE + LowE + lensing) spectra. In both cases, the red points lie close to the 3-σ contour border. Hence, when overplotting different fits, it will lead the observed tension of the Hubble parameter values from CMB and BAO [9,10] and also with the values

of Ω_m [80–83]. Moreover, the points in the $(\sigma_8 - h)$ plane also evince this discrepancy.

For the β-model, the situation is dramatically different when compared with the ΛCMD model as shown in Fig. 2. The related $(\sigma_8 - \Omega_m)$ plane exhibits the reduction of the point distances in the contours from 2-σ to roughly 1-σ contour. The related PDFs of β_0 and γ_0 parameters show the degeneracies of their values which may reduce even more
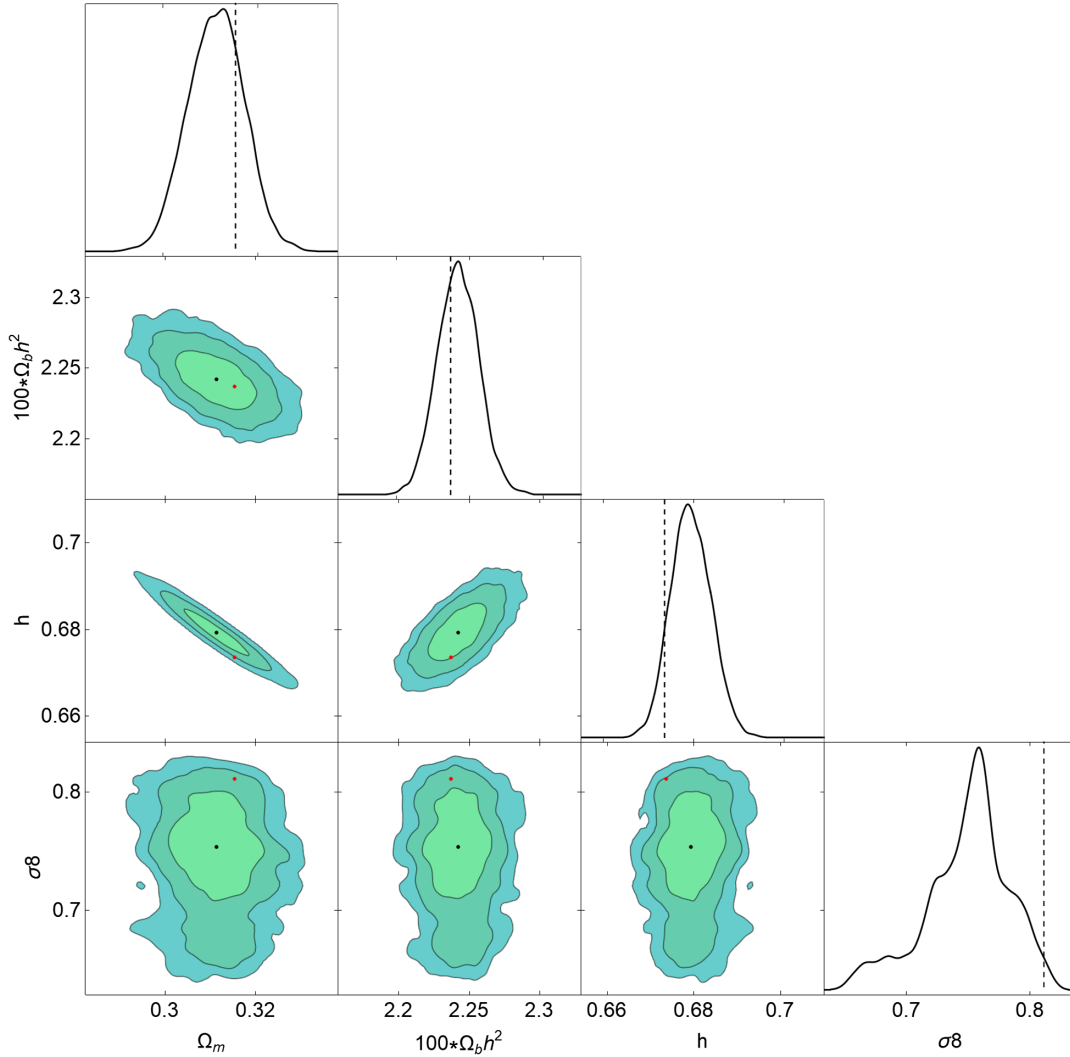
FIG. 1. Contour regions for ΛCDM at 1-σ, 2-σ and 3-σ with 68.3%, 95.4% and 99.7% confidence levels, respectively. Red points and vertical black dashed lines (in the PDF plots) connote the best-fit values from the CMB Planck 2018 data of the (TT, TE, EE + lowE + lensing) spectra. Black points refer to the median values of the parameters resulting from MCMC chains.
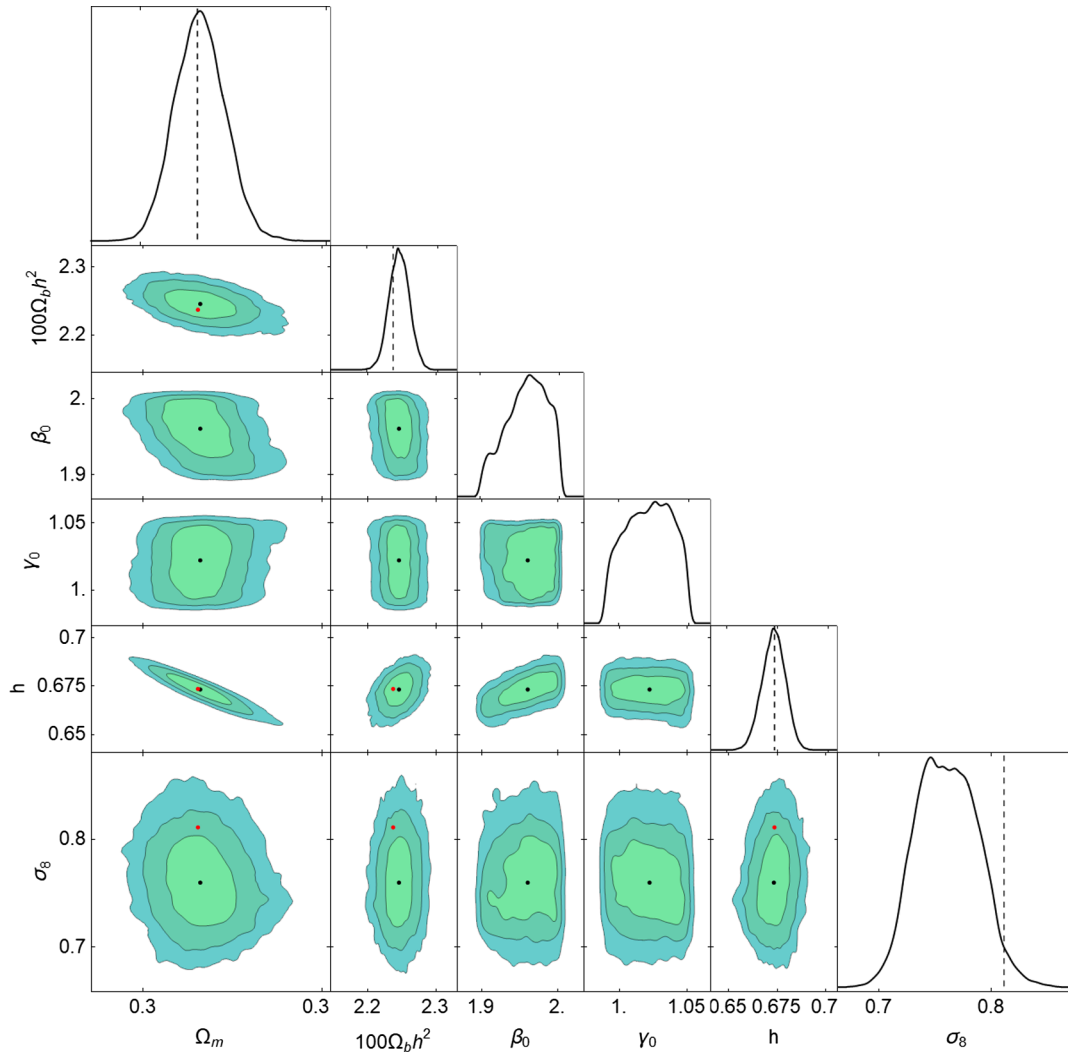
FIG. 2. Contour regions for the β-model for six parameters at 1-σ, 2-σ and 3-σ with 68.3%, 95.4% and 99.7% confidence levels, respectively. Red points and vertical black dashed lines (in the PDF plots) connote the best-fit value from the CMB Planck 2018 data of the (TT, TE, EE + lowE + lensing) spectra. Black points refer to the median values of the β-model parameters resulting from MCMC chains.

the point distances in the contours. Interestingly, on the contrary what happens in the aforementioned ΛCDM case, there is no discrepancy in the ($h - \Omega_m$) plane with a good accommodation of the parameters to data. On the other hand, in the ($\sigma_8 - h$) plane the best-fit values from the Planck 2018 lie at 2-σ contour. Hence, the overplotting contours from different fits will lead a mild discrepancy (tension) of data from different probes.

To complement the analysis, it is important to check the statistical relevance of the models as compared to observations. Most of the cosmology papers commonly adopt the AIC classifiers [84,85] as a first inference for model selection to estimate the difference between data fitting and particular models. The main idea is that the model with higher AIC tends to aggravate the tension between competing models (in a search of the "true" model compatible with observations) when more parameters are allowed.

The model with more free parameters is generally penalized accordingly. We first adopt the errors from the data regarded as Gaussian and use AIC to evaluate the fit to data for small sample sizes using the following expression:

$$\text{AIC} = \chi_{bf}^2 + 2k + \frac{2k(k+1)}{N-k-1}, \tag{71}$$

where χ_{bf}^2 is the best-fit χ^2 of the model (maximum likelihood), k represents the number of the uncorrelated (free) parameters and N is the number of the data point in the adopted dataset. The difference $|\Delta\text{AIC}| = AIC_{\text{model}(2)} - AIC_{\text{model}(1)}$ follows the Jeffreys' scale [86] that measures the intensity of the tension between two competing models and raises evidence against the complex one. Higher values for $|\Delta\text{AIC}|$ denote more tension between models and the more statistically uncorrelated they are. In this sense, we have

TABLE V. The obtained values of AIC and ΔAIC for the studied models as applied to the Jeffreys' scale.

Model	AIC	ΔAIC	Evidence against the model
ΛCDM	1096.33	0	Null
β-model	1100.42	4.09	Positive

that for $|\Delta\text{AIC} \leq 2|$ the models are statistically consistent with a considerable level of empirical support. For $4 < \Delta\text{AIC} < 7$ it indicates a positive tension against the model with a higher value of AIC. For $|\Delta\text{AIC} \geq 10|$ it defines a strong evidence against the model with a higher AIC. This criterion focuses on the penalty of free parameters which is an Occam's razor realization to avoid model complexity. Rather than just limiting the model classification to their parameters using AIC, the Bayesian evidence focuses on priors and seems to be a better tool to balance the model selection. Unfortunately, we were not able to numerically integrate the MCMC chains that revealed much sensitive to the choice of certain parameters. For the present application, we have the results of ΔAIC as shown in Table V that indicate a positive evidence against the β-model. This happens due to the fact that the β-model has two extra parameters when compared to ΛCDM.

As pointed out in [43,44], the analysis of the Jeffreys' scale from ΔAIC must be taken with caution to avoid misleading. It reveals a symptom of Jeffreys' scale sensitivity that can induce false positives or false negatives. This can be critical for cosmological models in which several probes of cosmic data present a significant level of tension between them, and the adoption of a complexity or over-simplified models is not a trivial task to decide [87–91]. On these terms, the results presented in Table V show that the β-model presents an additional unnecessary extra parameter. As indicated in Tables III and IV, the γ_0 parameter is tightly constrained by the MCMC chains with the value $\gamma_0 \sim 1$. This indication allows us to test the β-model setting $\gamma_0 = 1$ or equivalently setting the integration constant $k_0 = \frac{1}{\alpha_0}$ [see Eq. (34)]. This assumption still obeys the big bang nucleosynthesis constraints on G_{eff} of Eq. (39), i.e., $|G_{\text{eff}}/G_N - 1| \leq 0.2$ [92]. We stress that the ΛCDM/GR limit (i.e., $G_{\text{eff}} = G$) is obtained by the zeroth order of Taylor series on G_{eff}.

To run the code, we adopt the parameter vectors for the β-model as $\{\Omega_{m0}, 100\Omega_b h^2, h, \beta_0, \sigma_8\}$ for $\gamma_0 = 1$ as previously defined. Hence, we adopted the following priors $\{(0.001, 1), (0.001, 0.08), (0.4, 1), (1.9, 2.001), (0.1, 1.8)\}$. In Table VI, we present the results of the MCMC chains with the best-fit and median values in the first and second rows, respectively. Interestingly, the resulting contour plots in Fig. 3 show a slight overall improvement and a reduction of distance of the median values of the β-model and the Planck 2018 best-fit of σ_8 parameter. Hence, it may induce a decrease of tension when overplotting different contour fits of disjoint data. Moreover, the degeneracies on the β_0 parameter are still observed in the corresponding PDF panels. Hence, with only one extra parameter, as shown in Table VII, we have the results of ΔAIC values that indicate a weak evidence against the β-model. Moreover, a self-contained information can be obtained from the σ-distances D_σ [93] which are computed by

$$D_\sigma = \sqrt{2}\text{Inverf}\left[0, 1 - \Gamma\left(1, \frac{\Delta\chi^2}{2}\right)\right], \qquad (72)$$

where Inverf(x) is the inverse of the error function $\text{Erf}f(x)$ and $\Gamma(1, \frac{\Delta\chi^2}{2})$ is the incomplete gamma function, with $\Delta\chi^2 = \chi^2_{\text{model}(2)} - \chi^2_{\text{model}(1)}$. Taking the χ^2_{bf} values in Tables III and VI of the β-model with a different number of extra parameters, the resulting σ-distance $D_\sigma = 0.006$. It shows a very small distance indicating that the models are statistically equivalent, in other words, the γ_0 parameter can be set to 1 without loss of generality. Moreover, in Table VII, the resulting ΔAIC indicates that the β-model for just one extra parameter is preferred as compared to the ΛCDM model.

In Fig. 4, we compare the growth rate of the models and present the numerical plot of the growth density equation. By the quantity $\frac{\delta_m}{\delta_m(z=0)}$ in function of redshift z in Eq. (41), we use the median values presented in Table III and the growth-rate $f\sigma_8(z)$ data in Table II. In the panels, the solid line denotes the ΛCDM model and the dashed line represents the β-model pattern. In both cases, we have very close curves of the models with a slight superimposed β-model curve (with or without two extra parameters) over the ΛCDM curve.

TABLE VI. A summary of best-fit (first row) and median values (second row) of the background parameters calculated by using MCMC chains with the resulting χ^2 values for the β-model with five parameters. Errors were obtained directly from the covariant matrix of the MCMC chains. The results of χ^2_{red} and χ^2_{bf} were 0.973 and 1088.33, respectively.

Ω_{m0}	$100\Omega_{b0}h^2$	h	σ_8	Parameters
0.312 ± 0.006	2.244 ± 0.014	0.679 ± 0.005	0.762 ± 0.030	$\beta_0 = 1.991 \pm 0.023$
0.315 ± 0.004	2.245 ± 0.010	0.674 ± 0.004	0.764 ± 0.020	$\beta_0 = 1.965 \pm 0.017$
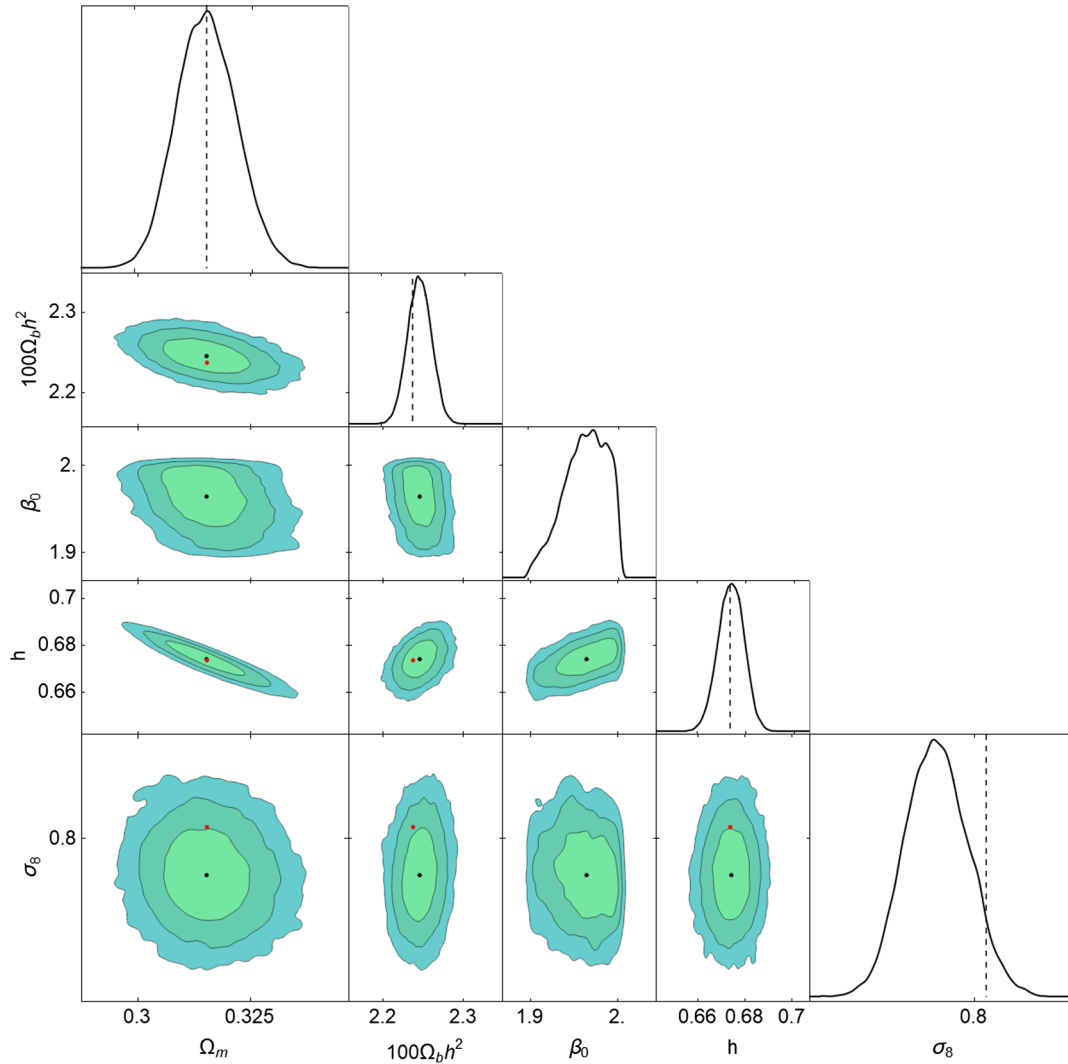
FIG. 3. Contour regions for the β-model with five parameters at 1-σ, 2-σ and 3-σ with 68.3%, 95.4% and 99.7% confidence levels, respectively. Red points and vertical black dashed lines (in the PDF plots) connote the best-fit value from the CMB Planck 2018 data of the (TT, TE, EE + lowE + lensing) spectra. Black points refer to the median values of the β-model parameters resulting from MCMC chains.

V. REMARKS

In this paper, using a geometric independent model based on the Nash-Greene embedding theorem we confronted the present model to the popular ΛCDM model through a joint analysis on recent pack of datasets on the CMB Planck collaboration, the Pantheon SNIa, BAO,

TABLE VII. The obtained values of AIC and ΔAIC for the studied models as applied to the Jeffreys' scale.

Model	AIC	ΔAIC	Evidence against the model
ΛCDM	1096.33	0	Null
β-model	1098.38	2.06	Weak

cosmic growth rate and the Hubble $H(z)$ evolution with addition of DES Y1 to BAO. We used a Markov chain Monte Carlo analysis (MCMC) from a modified MetropolisHastings algorithm to determine the cosmic parameters and found a nearly statistical equivalence at 1-σ contour with the ΔAIC values roughly around 2 between ΛCDM and the β-model with one extra parameter constrained by the data. Moreover, the observed distance discrepancy of best-fit points of the CMB Planck 2015 and the growth-rata data was reduced to the 1-σ contour limits when testing the β-model with the CMB Planck 2018 data. This situation may be improved with a reduction within the 1-σ contour by the appearance of the β-model degeneracy values consistent with the behavior of $f\sigma_8$. Motivated by the Jeffreys' scale, the β-model prefers only one extra parameter and with the addition of DES Y1 to the larger
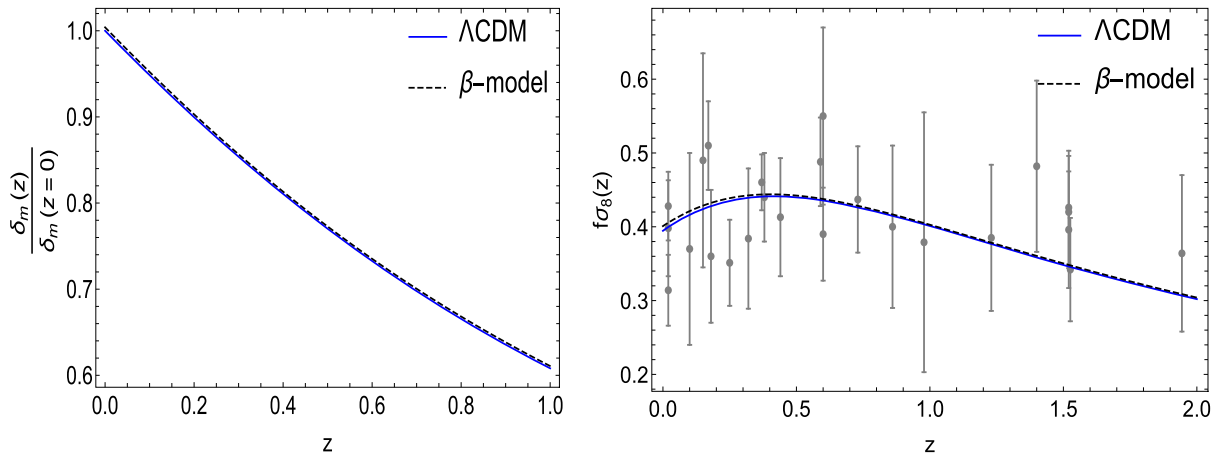
FIG. 4. Evolution on growth density equation (left panel) and the growth rate (right panel) of the considered models as a function of the redshift z.

dataset, and favors a better settlement of the cosmological parameters for this model and avoids overfitting. Moreover, the extra-parameter reduction does not compromise the ΛCDM/GR limit and the big bang nucleosynthesis constraints on G_{eff}. Hence, this turns the β-model capable of analyzing within a reasonable range of confidence level a more complete joint data apart from systematics for future datasets. As prospects, we intend to investigate the behavior of the viscosity parameter and growth-index rate and its signature on the integrated SachsWolfe (ISW) effect. This process is in due course and will be reported elsewhere.

[1] R. Decca, D. López, E. Fischbach, G. L. Klimchitskaya, D. E. Krause, and V. M. Mostepanenko, Eur. Phys. J. C **51,** 963 (2007).

[2] T. Jenke *et al.*, Phys. Rev. Lett. **112,** 151105 (2014).

[3] G. L. Klimchitskaya, Eur. Phys. J. C **77,** 315 (2017).

[4] G. Cronenberg, P. Brax, H. Filter, P. Geltenbort, T. Jenke, G. Pignol, M. Pitschmann, M. Thalhammer, and H. Abele, Nat. Phys. **14,** 1022 (2018).

[5] G. L. Klimchitskaya, V. M. Mostepanenko, R. I. P. Sedmik, and H. Abele, Symmetry **11,** 407 (2019).

[6] N. Arkani-Hamed, S. Dimopoulos, and G. Dvali, Phys. Lett. B **429,** 263 (1998).

[7] B. Riemann, Nature (London) **8,** 14 (1873).

[8] M. D. Maia, in *Geometry of the Fundamental Interactions* (Springer, New York, 2011), p. 166, https://doi.org/10.1007/978-1-4419-8273-5.

[9] P. A. R. Ade *et al.* (Planck Collaboration), Astron. Astrophys. **594,** A13 (2016).

[10] N. Aghanim *et al.* (Planck Collaboration), Astron. Astrophys. **641,** A6 (2020).

[11] R. J. Nemiroff, R. Joshi, and B. R. Patla, J. Cosmol. Astropart. Phys. 06 (2015) 006.

[12] B. Santos, A. A. Coley, N. Chandrachani Devi, and J. S. Alcaniz, J. Cosmol. Astropart. Phys. 02 (2017) 047.

[13] P. Kumar and C. P. Singh, Astrophys. Space Sci. **362,** 52 (2017).

[14] H. E. S. Velten, R. F. vom Marttens, and W. Zimdahl, Eur. Phys. J. C **74,** 3160 (2014).

[15] J. Sultana, Mon. Not. R. Astron. Soc. **457,** 212 (2016).

[16] N. Sivanandam, Phys. Rev. D **87,** 083514 (2013).

[17] K. Nozari, N. Behrouz, and N. Rashidi, Adv. High Energy Phys. **2014,** 569702 (2014).

[18] L. Randall and R. Sundrum, Phys. Rev. Lett. **83,** 3370 (1999).

[19] L. Randall and R. Sundrum, Phys. Rev. Lett. **83,** 4690 (1999).

[20] G. Dvali, G. Gabadadze, and M. Porrati, Phys. Lett. B **485,** 208 (2000).

[21] V. Sahni and Y. Shtanov, J. Cosmol. Astropart. Phys. 11 (2003) 014.

[22] A. Lue and G. D. Starkman, Phys. Rev. D **70,** 101501 (2004).

[23] K. Koyama, Phys. Rev. D **72,** 123511 (2005).

[24] M. Bouhmadi-López, J. Cosmol. Astropart. Phys. 11 (2009) 011.

[25] M. Bouhmadi-López and L. P. Chimento, Phys. Rev. D **82,** 103506 (2010).

[26] R. A. Battye and B. Carter, Phys. Lett. B **509,** 331 (2001).

[27] M. D. Maia and E. M. Monte, Phys. Lett. A **297,** 9 (2002).

[28] M. D. Maia, E. M. Monte, J. M. F. Maia, and J. S. Alcaniz, Classical Quantum Gravity **22,** 1623 (2005).

[29] M. D. Maia, N. Silva, and M. C. B. Fernandes, J. High Energy Phys. 04 (2007) 047.

[30] M. Heydari-Fard and H. R. Sepangi, Phys. Lett. B **649,** 1 (2007).

[31] S. Jalalzadeh, M. Mehrnia, and H. R. Sepangi, Classical Quantum Gravity **26,** 155007 (2009).

[32] M. D. Maia, A. J. S Capistrano, J. S. Alcaniz, and E. M. Monte, Gen. Relativ. Gravit. **43,** 2685 (2011).

[33] A. Ranjbar, H. R. Sepangi, and S. Shahidi, Ann. Phys. (Amsterdam) **327,** 3170 (2012).

[34] A. J. S. Capistrano and L. A. Cabral, Ann. Phys. (Amsterdam) **348,** 64 (2014).

[35] A. J. S. Capistrano, Mon. Not. R. Astron. Soc. **448,** 1232 (2015).

[36] A. J. S. Capistrano and L. A. Cabral, Classical Quantum Gravity **33,** 245006 (2016).

[37] A. J. S. Capistrano, A. C. Gutiérrez-Piñeres, S. C. Ulhoa, and R. G. G. Amorim, Ann. Phys. (Amsterdam) **380,** 106 (2017).

[38] A. J. S. Capistrano, Ann. Phys. (Berlin) **530,** 1700232 (2017).

[39] A. J. S. Capistrano, Phys. Rev. D **100,** 064049 (2019).

[40] J. Nash, Ann. Math. (N.Y.) **63,** 20 (1956).

[41] R. Greene, Am. Math. Soc. **97,** 63 (1970).

[42] X. Fan, N. A. Bahcall, and R. Cen, Astrophys. J. Lett. **490,** L123 (1997).

[43] S. Nesseris, G. Pantazis, and L. Perivolaropoulos, Phys. Rev. D **96,** 023542 (2017).

[44] C. A. Luna, S. Basilakos, and S. Nesseris, Phys. Rev. D **98,** 023516 (2018).

[45] R. Arjona, W. Cardona, and S. Nesseris, Phys. Rev. D **99,** 043516 (2019).

[46] D. M. Scolnic et al., Astrophys. J. **859,** 101 (2018).

[47] C. Zhang, H. Zhang, S. Yuan, S. Liu, T.-J. Zhang, and Y.-C. Sun, Res. Astron. Astrophys. **14,** 1221 (2014).

[48] D. Stern, R. Jimenez, L. Verde, M. Kamionkowski, and S. A. Stanford, J. Cosmol. Astropart. Phys. 02 (2010) 008.

[49] M. Moresco et al., J. Cosmol. Astropart. Phys. 08 (2012) 006.

[50] C. H. Chuang and Y. Wang, Mon. Not. R. Astron. Soc. **435,** 255 (2013).

[51] M. Moresco, Mon. Not. R. Astron. Soc. **450,** L16 (2015).

[52] T. Delubac et al. (BOSS Collaboration), Astron. Astrophys. **574,** A59 (2015).

[53] L. Samushia, W. J. Percival, and A. Raccanelli, Mon. Not. R. Astron. Soc. **420,** 2102 (2012).

[54] C. Howlett, A. Ross, L. Samushia, W. Percival, and M. Manera, Mon. Not. R. Astron. Soc. **449,** 848 (2015).

[55] M. Feix, A. Nusser, and E. Branchini, Phys. Rev. Lett. **115,** 011301 (2015).

[56] D. Huterer, D. Shafer, D. Scolnic, and F. Schmidt, J. Cosmol. Astropart. Phys. 05 (2017) 015.

[57] M. J. Hudson and S. J. Turnbull, Astrophys. J. **751,** L30 (2012).

[58] S. J. Turnbull, M. J. Hudson, H. A. Feldman, M. Hicken, R. P. Kirshner, and R. Watkins, Mon. Not. R. Astron. Soc. **420,** 447 (2012).

[59] M. Davis, A. Nusser, K. L. Masters, C. Springob, J. P. Huchra, and G. Lemson, Mon. Not. R. Astron. Soc. **413,** 2906 (2011).

[60] Y. S. Song and W. J. Percival, J. Cosmol. Astropart. Phys. 10 (2009) 004.

[61] C. Blake et al., Mon. Not. R. Astron. Soc. **436,** 3089 (2013).

[62] A. G. Sanchez et al., Mon. Not. R. Astron. Soc. **440,** 2692 (2014).

[63] C. Blake et al., Mon. Not. R. Astron. Soc. **425,** 405 (2012).

[64] A. Pezzotta et al., Astron. Astrophys. **604,** A33 (2017).

[65] T. Okumura et al., Publ. Astron. Soc. Jpn. **68,** 38 (2016).

[66] P. Zarrouk et al., Mon. Not. R. Astron. Soc. **477,** 1639 (2018).

[67] Héctor Gil-Marín et al., Mon. Not. R. Astron. Soc. **477,** 1604 (2018).

[68] J. Hou et al., Mon. Not. R. Astron. Soc. **480,** 2521 (2018).

[69] G.-B. Zhao et al., Mon. Not. R. Astron. Soc. **482,** 3497 (2019).

[70] T. M. C. Abbott et al., Phys. Rev. D **98,** 043526 (2018).

[71] T. M. C. Abbott et al., Mon. Not. R. Astron. Soc. **483,** 4866 (2019).

[72] H. Akaike, IEEE Trans. Autom. Control **19,** 716 (1974).

[73] S. K. Donaldson, Am. Math. Soc. **35,** 201 (1984).

[74] C. H. Taubes, Amer. Math. Soc. **35,** 493 (1984).

[75] C. S. Lim, Prog. Theor. Exp. Phys. **2014,** 2A101 (2014).

[76] A. B. Rivera and J. E. García-Farieta, Int. J. Mod. Phys. D **28,** 1950118 (2019).

[77] D. J. Eisenstein and W. Hu, Astrophys. J. **496,** 605 (1998).

[78] D. J. Eisenstein et al., Astrophys. J. **633,** 560 (2005).

[79] W. Sutherland, Mon. Not. R. Astron. Soc. **426,** 1280 (2012).

[80] E. Aubourg et al. (BOSS Collaboration), Phys. Rev. D **92,** 123516 (2015).

[81] S. Alam et al. (BOSS Collaboration), Mon. Not. R. Astron. Soc. **470,** 2617 (2017).

[82] E. Macaulay et al. (DES Collaboration), Mon. Not. R. Astron. Soc. **486,** 2184 (2019).

[83] G. Alestas, L. Kazantzidis, and L. Perivolaropoulos, Phys. Rev. D **101,** 123516 (2020).

[84] N. Sugiura, Commun. Stat. A **7,** 13 (1978).

[85] A. R. Liddle, Mon. Not. R. Astron. Soc. **377,** L74 (2007).

[86] H. Jeffreys, Theory of Probability, 3rd ed. (Oxford University Press, Oxford, 1961).

[87] A. R. Liddle, Mon. Not. R. Astron. Soc. **351,** L49 (2004).

[88] R. Trotta, Mon. Not. R. Astron. Soc. **378,** 72 (2007).

[89] M. Vardanyan, R. Trotta, and J. Silk, Mon. Not. R. Astron. Soc. **413,** L91 (2011).

[90] S. Nesseris and J. Garcia-Bellido, J. Cosmol. Astropart. Phys. 08 (2013) 036.

[91] M. Trashorras, S. Nesseris, and J. Garcia-Bellido, Phys. Rev. D **94,** 063511 (2016).

[92] C. J. Copi, A. N. Davis, and L. M. Krauss, Phys. Rev. Lett. **92,** 171301 (2004).

[93] J. C. B. Sanchez, S. Nesseris, and L. Perivolaropoulos, J. Cosmol. Astropart. Phys. 11 (2009) 029.